Astron. Astrophys. 274, 279–290 (1993)

ASTRONOMY AND ASTROPHYSICS

Colour evolution models and the distribution of LMC clusters in the integrated UBV plane

L. Girardi and E. Bica

Instituto de Física – UFRGS, Caixa Postal 15051, 91540-000 Porto Alegre RS, Brazil

Received December 2, 1992; accepted February 23, 1993

Abstract. We present a comparison between photometric cluster models, based on classical and with-overshooting stellar tracks, and the enlarged sample of 624 LMC clusters recently gathered in integrated UBV photometry by Bica et al. Models based on Maeder and Meynet's tracks present two temporary red phases: the first at age 10 Myr, caused by a clump of red supergiants; the second at $\sim$ 100 Myr due to the combined effect of both the progressive reduction of the blue loop of core He-burning stars, and their fading relative to top-MS stars. The 100 Myr red phase does not occur in models without overshooting.

Taking into account stochastic effects on the mass distribution of stars, the models describe well the general distribution of clusters in the $(U-B)$ vs. $(B-V)$ diagram, except for the oldest, SWB types V-VII, clusters. The dispersion of cluster colours due to stochastic effects is found to be strongly variable along the ageing sequence: the general trend is a decrease with age due to the increasing population of post-MS phases, but the dispersion increases in the temporary red phases and is expected to increase again after the red giant branch phase transition due to the appearance of extended RGBs and carbon stars. We also study the LMC clusters age distribution function, based on the age frequency of clusters of equal initial masses, taking into account different values for the IMF slope.

Key words: galaxies: Magellanic Clouds – stars: evolution of – stars: HR diagram – galaxies: star clusters

1. Introduction

As a stellar population ages, it becomes redder due to the loss of top main sequence (top-MS) stars. This simple evolutionary path to the lower right corner of the integrated $(U-B)$ vs. $(B-V)$ diagram is however disturbed due to changes on the distribution of post-MS stars. The most conspicuous features are the appearance of temporary red loops (Arimoto & Bica 1989), as well as some changes on the rates at which the colours evolve.

This colour evolution of stellar populations has been the subject of several recent works, such as Renzini & Buzzoni (1986), Charlot & Bruzual (1991). A primary aim of these models is the reproduction of the observed integrated properties of single burst populations (i.e. clusters). Such a comparison with the integrated colours of LMC clusters has been the main subject of the works by Chiosi et al. (1988, hereafter CBB88), who considered in detail the possible explanations for the bimodal distribution of $(B-V)$ colours, and Alongi & Chiosi (1989), who studied ages and total masses of LMC clusters based on their integrated UBV photometry. Such photometric masses for a large number of clusters can be checked with direct mass determinations available for some clusters (e.g. Dubath et al. 1990; Fischer et al. 1992a, 1992b). Arimoto & Bica (1989) reproduced the colours of clusters with red supergiants (RSGs) by including tracks for massive stars and suitable time steps.

The integrated UBV sample used in previous LMC studies was that of van den Bergh (1981) with 147 clusters, in some cases complemented with Mateo's (1988a) sample of 31 clusters in an outlying field. Recently, Bica et al. (1991, 1992a, hereafter BCDSP) extended the sample of LMC clusters with available UBV integrated photometry to a total of 624 objects. Their sample includes fainter clusters, being basically complete up to $V \simeq 13.2$ (Bica et al. 1992b).

In the present paper we discuss the BCDSP data in the light of simple colour evolution models. We consider both classical and overshooting stellar tracks, and different IMF slopes. Integrated models based on Castellani et al. (1992, hereafter CCS92) and Maeder & Meynet (1991, hereafter MM91) isochrones are presented in Sect. 2, being their differences considered in detail. Section 3 deals with the comparison with the observational data, presenting the derivation of the LMC clusters age distribution based on BCDSP data. Stochastic effects on the IMF are tested as the main source of dispersion of clusters on the integrated $(U-B)$ vs. $(B-V)$ diagram. Section 4 summarizes the main results and presents the final considerations.

2. Photometric models

There are several possible approaches to the problem of evolutionary population synthesis, as described by Charlot & Bruzual (1991). Here we will use that adopted by these authors, deriving

Send offprint requests to: L. Girardi

the UBV integrated colours of clusters directly from theoretical isochrones.

To clarify the notation, lowercase m refers to stellar initial masses, while caligraphic $\mathscr{M}$ will refer to cluster total masses. All masses are given in $M_\odot$ units. The age of stars or clusters given in units of years is denoted by t.

2.1. Isochrones

The models were computed with two different sets of isochrones. The MM91 isochrones, obtained from stellar evolutionary tracks with moderate convective overshooting, mass loss and solar metallicity (Y = 0.28, Z = 0.02), cover the mass range $120 - 0.8 M_\odot$. CCS92 isochrones were obtained from classical (i.e. without mass loss and overshooting) tracks with Z = 0.02 and Y = 0.27, on the range $9 - 0.6 M_\odot$. Additional isochrones for Z = 0.006 and both Y = 0.23 and Y = 0.27 were kindly made available by Dr. Castellani. Both sets of stellar tracks were obtained with the same opacity tables and nuclear reaction rates.

For both sets of isochrones, the ZAMS was extended down to 0.15 $M_\odot$ using VandenBerg et al. (1983) low-mass star models and the empirical bolometric corrections and colours from Johnson (1966).

In MM91, the evolutionary tracks for massive stars extend up to the pre-supernova stage, which allows one to check the effect of red and blue supergiants on the integrated colors. The intermediate masses include evolution up to the early asymptotic giant branch (E-AGB) end, whereas the low-mass stars stop at the He-flash (Maeder & Meynet 1989, hereafter MM89). As the contribution of termally pulsing AGB (TP-AGB) stars to the integrated light and optical colours of younger clusters is not significant (see e.g. Figs. 4 and 8 of Charlot & Bruzual 1991), the integrated models are then essentially complete in evolutionary phases up to ages $\sim$ 2.5 Gyr. For older isochrones all the He-burning phases are lacking, and so we prefer not to take any conclusion from them.

In the CCS92 isochrones the situation is quite complementary: although they do not include massive stars, the low- and intermediate-mass tracks are complete until the E-AGB end. So, an interesting comparison is possible between with- and without-overshooting models for clusters with evolved intermediate-mass stars.

Although most models presented here have solar metallicity, it will be shown in Sect. 2.3.2 that they are a reasonable approximation for ages lower than $\sim$ 2 Gyr in the LMC. For older ages, lower metallicity models are necessary.

It is important to certify that the transformations from the theoretical ($L_{\rm bol}, T_{\rm eff}$) to the observed ($M_V, B-V$) plane are the same for the different stellar models used. The good agreement between the CCS92 and MM91 without-overshooting isochrones ensures that the bolometric corrections and $T_{\rm eff}$ vs. $(B-V)$ relations adopted by the different authors are basically the same. So, any difference between colours calculated from the two sets of isochrones should be attributed only to the different physical inputs – mainly to the presence of overshooting and mass loss on MM91 models – and not to differences in the bolometric corrections and colour relations applied to the stellar model results.

With this in mind, we applied to CCS92 isochrones the same $(U-B)$ vs. $(B-V)$ relations from Schmidt-Kaler (1982) which were adopted in MM91. Different relations were applied to dwarfs, giants and supergiants stars. Although in Maeder and Meynet's work the transition between giants and supergiants was chosen at the RGB tip, we prefered to adopt a different approach: we considered all post-MS stars fainter than $M_V = -4$ as giants, and all brighter than $M_V = -5$ as supergiants, with a smooth transition between these limits. So, the attributed luminosity classes are in agreement with those of solar vicinity stars, which originated the adopted $(U-B)$ vs. $(B-V)$ relations. The MM91 isochrones were also modified accordingly. However, this modification does not affect significantly the results presented below.

2.2. The IMF

The formalism of star cluster integrated models is presented in e.g. Alongi & Chiosi (1989). Given an isochrone of age t, the cluster integrated luminosities can be calculated by the simple integration:

$$L_{T\lambda}(t) = \int_0^\infty \phi_m L_{\lambda t}(m) {\rm d}m \ , \qquad (1)$$

being ϕ_m the IMF in terms of the number of stars in the mass interval $[m, m+{\rm d}m]$, and $L_{\lambda t}(m)$ the luminosity in the λ bandpass of a star of mass m. The U, B and V integrated luminosities can be easily converted to colours and magnitudes.

Here we adopted a Salpeter-like IMF, $\phi_m \, \alpha \, m^{-(x+1)}$, for the entire mass interval. IMF slopes x = 2.5 and 1.35 were considered. These values encompass results from recent CCD data for LMC clusters (Mateo 1988b and Richtler et al. 1991). Although there is evidence in the solar vicinity of a bimodal IMF slope (e.g. Miller & Scalo 1979; Scalo 1986), this effect is minor when we refer to the *colour* of a cluster. As will be seen, the integrated colour of a cluster depends mainly on the ratio between top-MS and post-MS luminosities. As the mass difference between stars in these stages is not large compared to the entire mass spectrum, the mass spectrum for these stars can be well represented by a single IMF slope, and the cluster colours marginally depend on its value. In young clusters this might not be totally true because the differences in mass and colours between top-MS and post-MS stars are larger than in intermediate age clusters.

A convenient way to present the results of Eq. (1) is on the form of luminosities and magnitudes per unit of cluster initial mass. So, the IMF is normalized so that

$$\int_{m_{\rm l}}^{m_{\rm u}} m \phi_m {\rm d}m = 1 \ M_\odot \ . \qquad (2)$$

While an upper limit $m_{\rm u}$ = 100 $M_\odot$ is a natural choice, the lower limit $m_{\rm l}$ is critical because it will determine the mass-to-light ratios for the models. We chose $m_{\rm l}$ values in order to

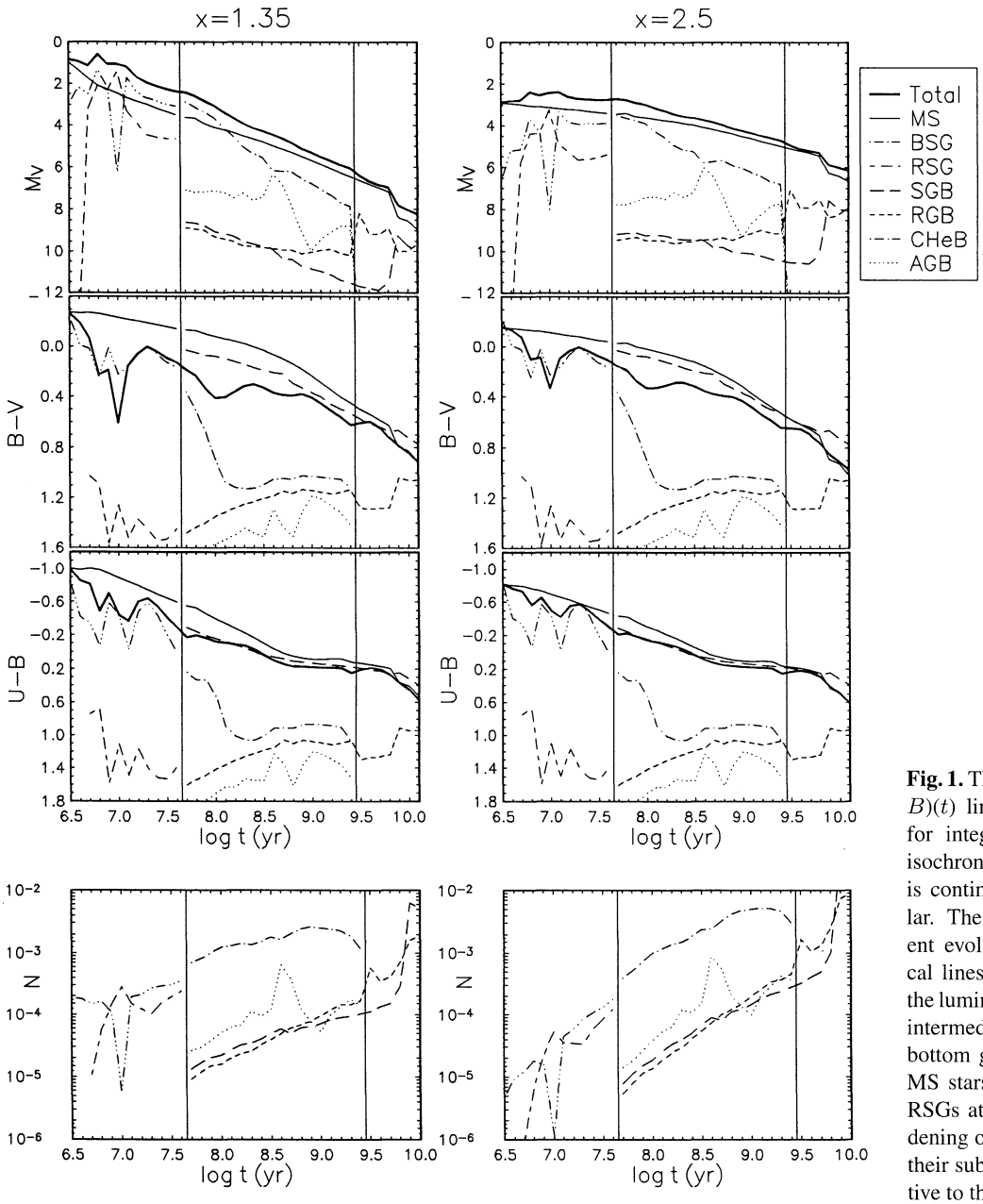

Fig. 1. Theoretical M_V, $(B-V)$ and $(U-B)(t)$ lines per unit cluster initial mass, for integrated models based on MM91 isochrones. The mass distribution of stars is continuous and the composition is solar. The contribution of stars in different evolutionary phases is shown. Vertical lines limit the age intervals in which the luminosities are dominated by massive, intermediate-mass and low-mass stars. The bottom graphs show the number of post-MS stars. Notice the sudden presence of RSGs at $t = 10^7$ yr, the progressive reddening of the CHeB stars until 10^8 yr, and their subsequent luminosity decrease relative to the MS

reproduce the mean value $\mathscr{M}/L_V = 0.2$ determined observationally for MC clusters of age $t \simeq 10^8$ yr (see Fig. 4 in Battinelli & Capuzzo-Dolcetta 1989). These values are $m_{\rm l} = 0.039\ M_\odot$ for $x = 1.35$ and $m_{\rm l} = 0.57\ M_\odot$ for $x = 2.5$. Under these assumptions it is possible to estimate cluster masses by comparing their observed luminosities with theoretical ones. It is also important to stress that the $m_{\rm l}$ values are used only in the IMF normalisation (Eq. 2), whereas integrated luminosities refer to stars distributed over the entire $100 > m(M_\odot) > 0.15$ interval.

2.3. *The behaviour of the models*

The models presented in this section correspond to the evolution of "superpopulous clusters"; i.e. the isochrones are continuously populated, even in the fast evolutionary phases, which eliminates stochastic effects on integrated colours and magnitudes (see Sect. 3.2). In practice, it means that these clusters have initial masses higher than $\sim 10^7\ M_\odot$.

In Figures 1 and 2 we present the obtained UBV colours and magnitudes per unit cluster mass (Eq. 2), for models based, respectively, on MM91 and CCS92 isochrones. Notice that the $M_V(t)$ curve position depends on the $m_{\rm l}$ choice, and with the present one curves with different xs intersect at $\log t \simeq 8$. We can see also the contribution to the integrated magnitudes from stars in different evolutionary phases. In young clusters the evolved stars were classified as blue or red supergiants (BSG and RSG, Fig. 1). In intermediate-age and old clusters the main evolved phases – namely, the subgiant branch (SGB), the red

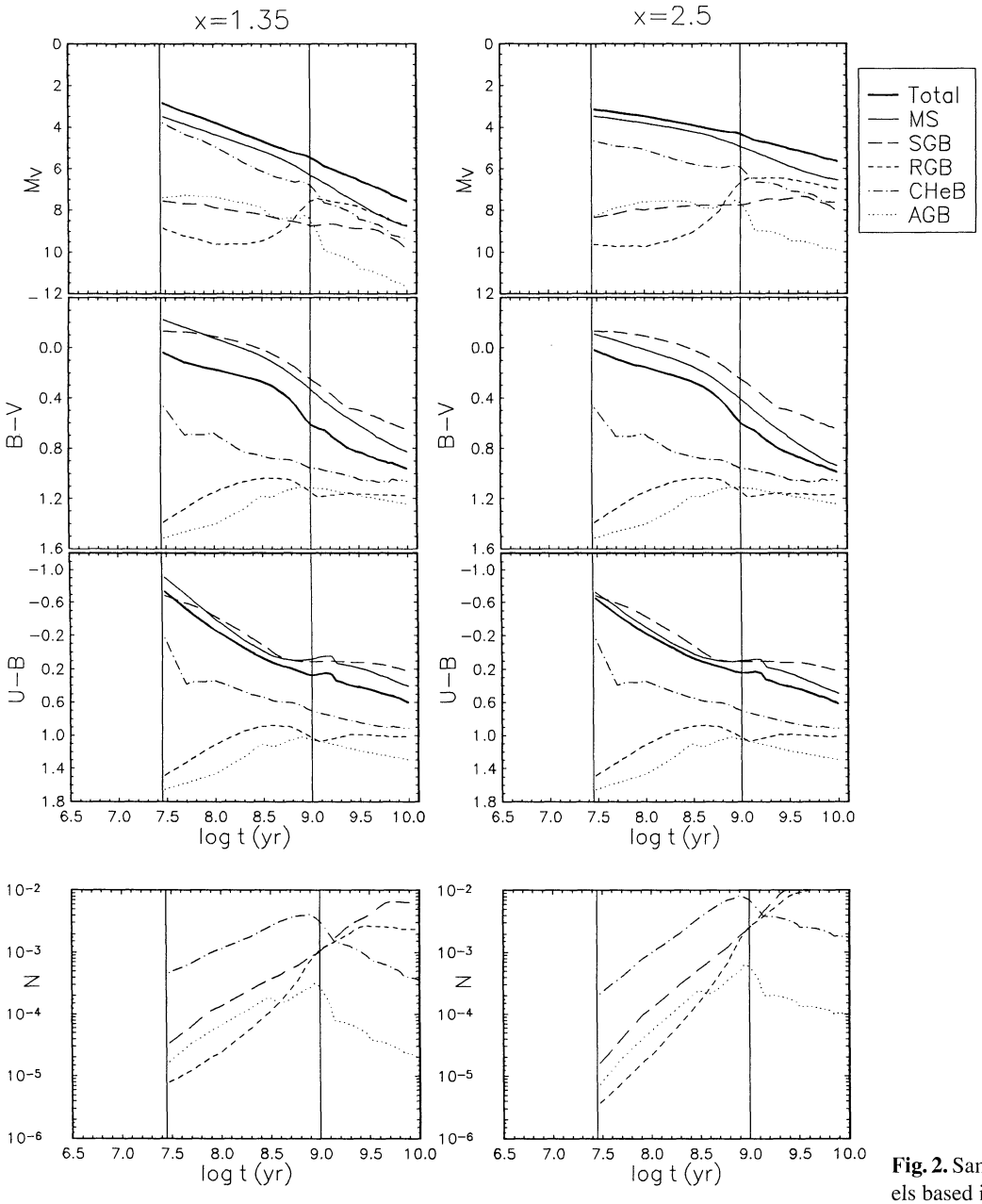

Fig. 2. Same as Fig. 1 but for integrated models based in CCS92 $Z = 0.02$ isochrones

giant branch (RGB), the core He-burning phase (CHeB) and the asymptotic giant branch (AGB) – are separated (Figs. 1 and 2).

The integrated models we calculate correspond to instantaneous burst populations. The assumption of a finite burst length (of $\sim 10^6$ to 5×10^6 yr) would affect only the very young clusters (of ages $t \lesssim 10^7$ yr), smoothing the evolutionary lines presented in Figs. 1 and 2. After 10^7 yr the results would be essentially the same as those obtained for instantaneous bursts.

2.3.1. MM91 integrated models

In Figure 3 the models based on MM91 isochrones, reddened by the Galactic foreground $E(B-V) = 0.06$, are superimposed on the observed $(U-B)$ vs. $(B-V)$ diagram for LMC clusters. Some interesting features in the models have counterparts in the cluster distribution:

1) There is an extended loop to the red at $t = 10^7$ years, due to the sudden clustering in the HR diagram of massive supergiants as RSGs. This phase is linked to two of the limiting masses that define different evolutionary sequences for massive stars (MM89). After the RSG phase, stars slightly more massive than $m_{\rm WR} \simeq 40\ M_\odot$ lose enough mass so that they become blue even before ending central He-burning, going rapidly to the WR stage and SN explosion, while stars below this mass limit start burning helium as RSGs and undergo SN explosion still as RSGs. At the age when the turn-off mass $m_{\rm TO}$ attains $m_{\rm WR}$, the cluster moves suddenly to the red. However, stars less massive than $m_{\rm Ceph} \simeq 12\ M_\odot$ develop an extended blue loop in which most of helium is burned, and which intersects

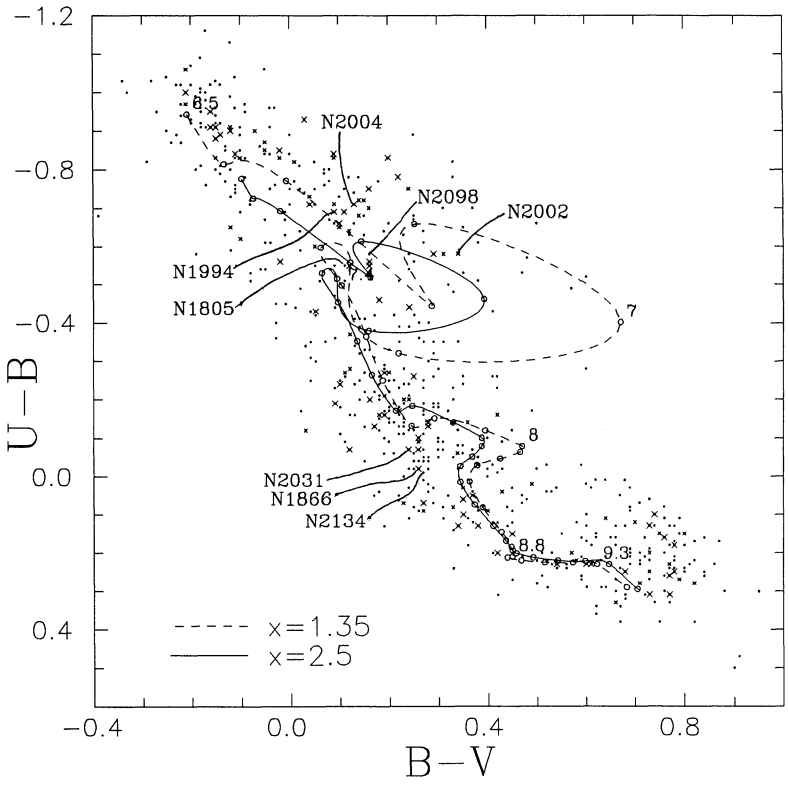

Fig. 3. The cluster models based on MM91 isochrones, reddened by $E(B-V) = 0.06$, are superimposed on the observed $(U-B)$ vs. $(B-V)$ diagram. More massive clusters are denoted by $\times$s. Circles along the lines are at $\Delta \log t = 0.1$ age intervals. Some particular values of $\log t$ are labeled

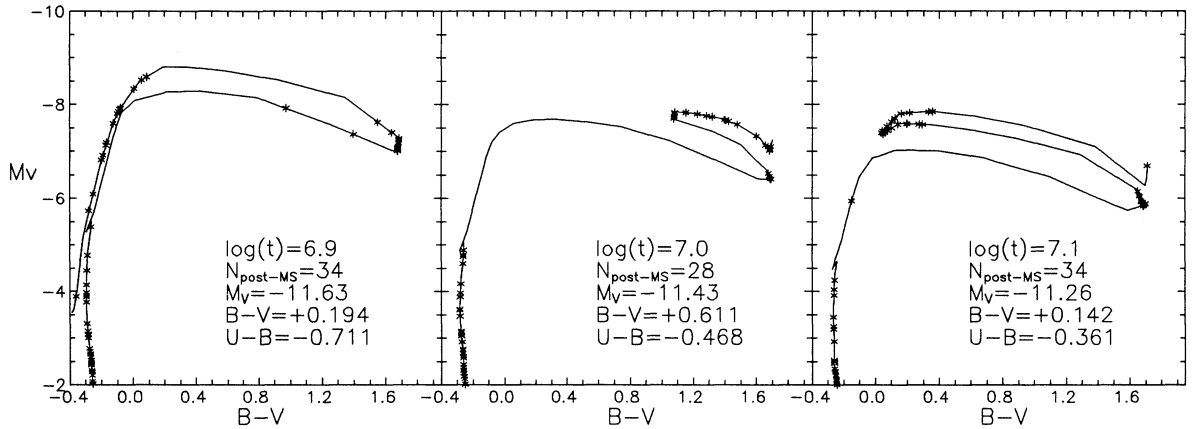

Fig. 4. The development of the RSG phase from $\log t = 6.9$ to 7.1, shown for a synthetic cluster with initial mass $\mathcal{M} = 10^5\ M_\odot$. In this example we have an $x = 1.35$ IMF slope. The synthetic HR diagrams are superimposed on the MM91 isochrones

the Cepheid instability strip. These blue core He-burning stars cause the cluster to move back to the blue when $m_{\rm TO}$ attains $m_{\rm Ceph}$. Figure 4 shows, with the aid of synthetic HR diagrams, the development of this red phase, hereafter called *RSG phase*.

The RSG phase lasts for the period of time in which $m_{\rm WR} > m_{\rm TO} > m_{\rm Ceph}$. As the $m_{\rm WR}$ value is highly dependent on the adopted mass loss rates, which are anyway still uncertain, it is not yet safe to derive the theoretical duration of the RSG phase. Otherwise, the stellar model grids do not offer enough number of tracks to set definite bounds on the limiting masses. In the present models, the RSG phase occurs between ages 8 and 13 Myr.

The presence of the RSG phase is well documented and can be clearly seen in the integrated spectra of the LMC clusters NGC 1805, NGC 1994, NGC 2002, NGC 2004 and NGC 2098 (Bica et al. 1990, hereafter BAS90). These clusters (Fig. 3) are shifted to the blue in comparison with the model loop. This is certainly due to the fact that the model has a higher metallicity than that of the LMC clusters. Also, as compared with the clusters observed in the RSG phase, the extension of the loop clearly favours the IMF slope $x \simeq 2.5$ – at least for the massive stars, which dominate the luminosity in these young clusters.

2) Another red loop occurs in the model at $t \sim 10^8$ yr. The reasons for this second loop are more subtle: the evolution to the red between $\log t \simeq 7.7$ and 8.0 is mostly due to the progressive

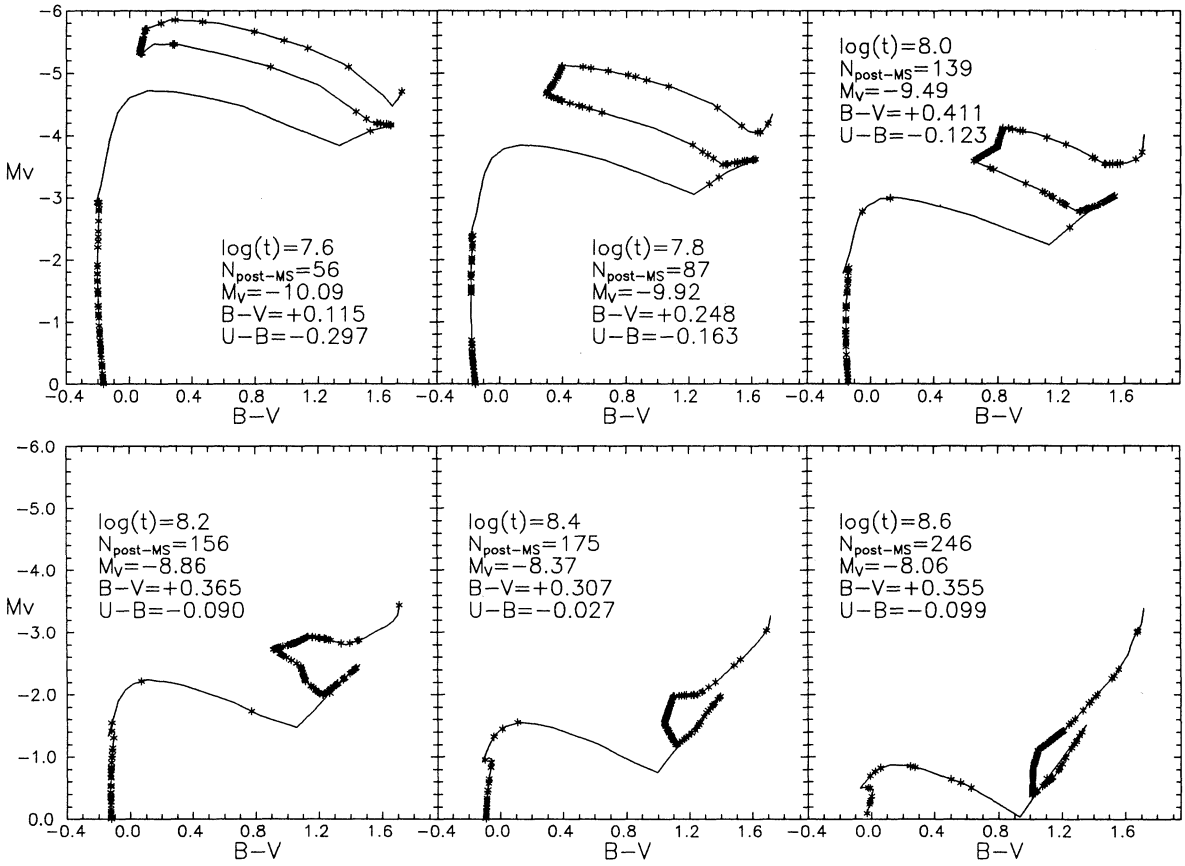

Fig. 5. The development of the 100 Myr red phase from $\log t = 7.6$ to 8.6, shown for a cluster with initial mass $\mathcal{M} = 10^5\ M_\odot$ and $x = 1.35$

reduction of the blue extension of the core He-burning phase. By 10^8 yr the CHeB is already concentrated in a red clump (the horizontal branch, HB), whose luminosity is afterwards progressively reduced in comparison with the blue top-MS stars. It causes the return of the cluster to the blue between $\log t \simeq 8.0$ and 8.3. This sequence, hereafter called *100 Myr red phase*, is illustrated in Fig. 5.

A similar red phase was observed in the integrated spectra of NGC 1866, NGC 2031 and NGC 2134 (BAS90). It was previously suggested as being due to the presence of intermediate-mass AGB stars, as denoted by the M giants observed in NGC 1866 (LMC) and NGC 2516 (Galactic), which appear to be responsible for the strong TiO bands in the integrated spectra. The present models suggest that an additional effect envolving slightly hotter stars contributes to this colour change: the reduction of the blue excursion of CHeB stars, accompanied by their fading relative to the top-MS.

As the MM91 isochrones lack the He-burning phases for low-mass stars, they are not appropriate for describing the evolution of clusters older than $\log t = 9.4$ (2.5 Gyr).

2.3.2. CCS92 integrated models

The most striking difference between MM91 and CCS92 integrated models is exactly the lack of the 100 Myr red phase in the latter (Fig. 6). In both sets of stellar models the ratio between the time spent in H and He burning, $t_{\rm He}/t_{\rm H}$, is almost the same for intermediate-mass stars, ~ 0.25. However, there are three main differences on the CHeB morphology that can be responsible for this different behaviour:

i) As the CHeB starts at higher He core masses in overshooting models, it also occurs at higher luminosities.

ii) In overshooting models the blue extension of the CHeB phase is shorter than in classical models. In this case, this difference amounts to $\Delta \log T_{\rm eff} \sim 0.08$, or as much as $\Delta(B-V) \sim 0.4$ (partly due to the use of different $T_{\rm eff}$ vs. $(B-V)$ relations). However, this difference occurs only for intermediate-mass stars, whereas for low-mass stars the CHeBs have similar $T_{\rm eff}$s.

iii) The transition of the CHeB loop to a red HB clump occurs later and more gradually for classical models.

These points have been discussed by Bertelli et al. (1985). The main physical parameter determining the CHeB morphology, as well as its time evolution, is the dependence of the helium core mass at He-ignition on the initial stellar mass. Items i) and iii), which are apparent in the comparison of Figs. 1 and 2, are determinant for the appearance of the 100 Myr red phase, while item ii) concerns mostly to its colour extension. We point out that the 100 Myr red phase occurs only in models with overshooting. It would be important to further discuss this age interval, investigating in detail the roles of overshooting and mass loss.

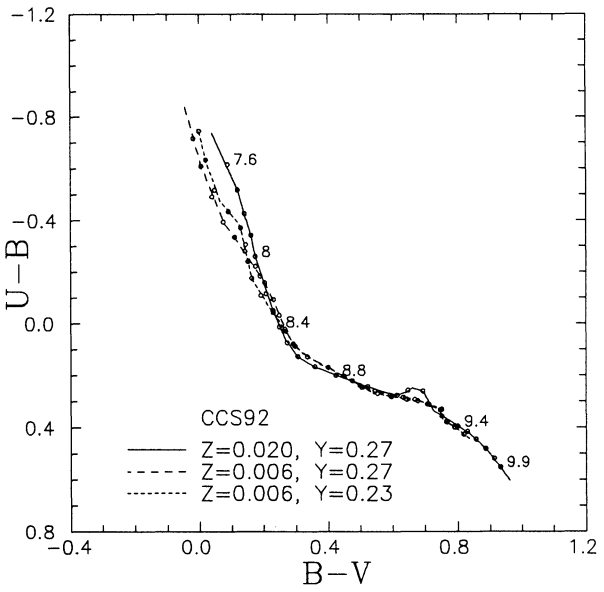

Fig. 6. The evolutionary paths of cluster models based on CCS92 isochrones on the $(U-B)$ vs. $(B-V)$ diagram, for an $x = 1.35$ IMF slope. Points are marked at $\Delta \log t = 0.1$ age intervals. Some particular values of $\log t$ are labeled for the $Z = 0.02$ model

As the observational evidence of red phases is stronger in the near infrared spectra (BAS90), a full discussion would better include the calculation of synthetic colours as $V-K$, $V-I$, etc.

We recall that CBB88 integrated models, which used a prescription for convective overshooting different from that of MM89, also do not show the 100 Myr red phase. The probable reason for this difference is that in Chiosi et al. tracks the blue extension of the CHeB occurs at much lower temperatures than in MM89 ones (see Fig. 21 of MM89 for a comparison), and so the time evolution of the CHeB does not cause a rapid change in the integrated colours of their cluster models. In addition, CBB88 stellar models present a significantly lower $t_{\rm He}/t_{\rm H}$ ratio, ~ 0.1 for intermediate-mass stars. MM89 adjusted their overshooting scale in order to reproduce, among other observational constraints, also the blue extension of the CHeB for Galactic clusters; so their tracks reproduce more satisfactorily the features responsible for the occurrence of the 100 Myr red phase (see, however, Alongi et al. 1991).

The CCS92 integrated models are not suitable to describe the hook at $(B-V) \simeq 0.8$ of older clusters. The hook would be well reproduced only by models with metallicity as low as $Z \simeq 10^{-3}$ (see Alongi & Chiosi 1989): these low metallicity stars not only develop a blue horizontal branch, but are also intrinsically bluer than solar metallicity stars due to their lower atmospheric opacities. However, we can see in Fig. 6 that the $Z = 0.006$ older models already show a clumping at $(B-V) \simeq 0.8$, which is a first step for the development of the hook.

The small difference between the CCS92 integrated models for $Z = 0.02$ and $Z = 0.006$ (Fig. 6) suggests that the comparison of LMC young clusters with solar metallicity models is reasonable. We note that the same $(B-V)$ vs. $(U-B)$ relations, obtained from solar metallicity stars, were applied to all the isochrones. We tried to estimate the error introduced in the integrated colours by this approach by comparing the Buser & Kurucz's (1978) theoretical bolometric corrections and $T_{\rm eff}$ vs. colours relations obtained for model atmospheres with solar ($\log A = 0$) and 1/10 solar ($\log A = -1$) metallicities. For the same values of $T_{\rm eff}$ and surface gravity g, models with $T_{\rm eff} > 8000$ K ($B-V < 0.1$) essentially do not differ in their colours. In the interval $8000 > T_{\rm eff}({\rm K}) > 5500$ ($0.1 < B-V < 0.7$), $\log A = -1$ models are bluer by, at most, ~ 0.06 in $(B-V)$ and ~ 0.2 in $(U-B)$. The bolometric corrections are typically 0.04 mag larger in $\log A = -1$ models, being this difference almost independent of the $T_{\rm eff}$ and g values. Considering that young LMC clusters present typical abundances from 1/2 solar to solar, we estimate that the errors in the integrated colours for our young models cannot exceed ~ 0.03 in $(B-V)$ and ~ 0.1 in $(U-B)$, in the sense that the models are redder. For intermediate-age clusters, as well as for young clusters in the RSG phase, in which cooler stars have an important contribution to the integrated colours, we compared the position of the features in CM diagrams for clusters of different metallicities. For instance, the Sandage (1988) composite CM diagrams for low ([Fe/H]~ -0.6) and high ([Fe/H]~ 0) metallicity Galactic intermediate-age clusters differ of ~ 0.05 in $(B-V)$ for the MSs, and of ~ 0.1 for the RGBs and HB clumps. With respect to RSGs, in Mermilliod's (1981) composite CM diagrams for Galactic young clusters the RSG clumps are separated from the upper-MS by $\Delta(B-V) \simeq 1.90 - 2.05$, whereas this difference amounts to ~ 1.85 for the LMC cluster NGC 2004 (see Sagar et al. 1992). As an extreme case, in the low metallicity ([Fe/H]~ -1.3) SMC cluster NGC 330 this difference is ~ 1.5 (see Carney et al. 1985). All these differences for individual stellar types would imply, in the integrated models, in a shift $\Delta(B-V) \lesssim 0.1$ in all cases.

2.3.3. Comparison with Bruzual & Charlot models

Bruzual & Charlot (1993) computed integrated models based on the same MM89 tracks, and complementing the low-mass stellar tracks with the He-burning phases. Figure 7 compares their model with ours, for the same $x = 1.35$ IMF. Essentially the same features are seen in both models, in particular the RSG and 100 Myr red phase are clearly present. However, Bruzual & Charlot models are slightly bluer, which could be attributed to the use of different interpolation algorithms in the isochrone construction, and/or different empirical bolometric corrections and colour relations. Their models extend to $(B-V) \simeq 1.0$ because they computed old clusters.

3. Comparison with BCDSP observations

In the present section the discussion is based on the MM91 integrated models, because they include the evolution of very young clusters. The presence of the 100 Myr red phase will also be important for the reproduction of the observed dispersion of clusters seen in Fig. 3.

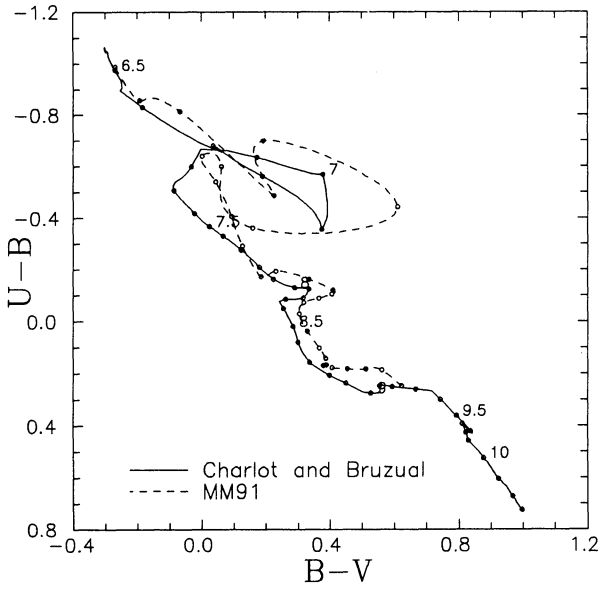

Fig. 7. Same as Fig. 6, but comparing ours and Bruzual & Charlot (1992) integrated models, both based on MM89 tracks

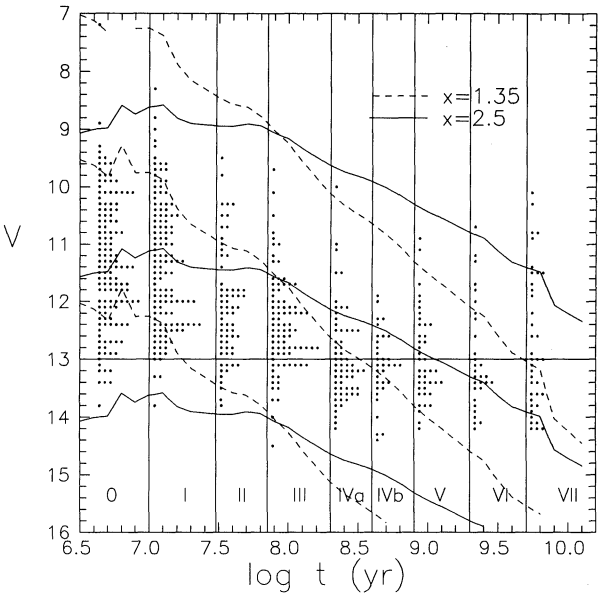

Fig. 8. Theoretical fading lines for initial masses 10^3, 10^4 and 10^5 $M_\odot$, superimposed on the observed plane V vs. $\log t$. The horizontal line indicates the magnitude $V = 13$ above which the sample is basically complete. Vertical lines are the limits to the age bins adopted by BCDSP, with the corresponding SWB types indicated

3.1. Age distribution of LMC clusters

We can associate an age t to each cluster, according to its position on the $(U-B)$ vs. $(B-V)$ diagram. The scale is given by the few clusters with age determined by their HR diagrams (Elson & Fall 1985). Bica et al. (1991) followed this procedure, classifying the LMC clusters into age bins, in a classification scheme equivalent to the SWB (Searle et al. 1980). The former classification differs from that of SWB by the inclusion of a "SWB 0" group (clusters younger than 10 Myr) and by splitting group IV into IVa and IVb. So, to each cluster we attribute the mean age of its age bin. Then the BCDSP data can be used to derive the age distribution function (ADF) of LMC clusters, providing statistically more significant ADFs with respect to previous attempts based on smaller samples.

In order to derive the cluster ADF, we must isolate the clusters with the same initial total masses. The initial "photometric" mass $\mathscr{M}$ of a cluster of age t is given by:

$$\mathscr{M} = 10^{0.4[M_V(t)-V+(m-M)]}\ , \qquad (3)$$

being V the observed visual magnitude, $M_V(t)$ the theoretical fading line for each $M_\odot$ of the initial cluster mass, and $(m-M) = 18.7$ the distance modulus of the LMC. This photometric mass depends on the m_l value adopted for calculating $M_V(t)$. Assuming that the clusters have the same IMF, Eq. (3) provides a *relative* scale of cluster initial masses.

In Figure 8 a set of theoretical fading lines for $\mathscr{M} = 10^3$ to 10^5 $M_\odot$, and $x = 1.35$ and 2.5, are superimposed on the data in the plane V vs. $\log t$. The revised SWB types divide the age sequence in age bins, while the fading lines for different $\mathscr{M}$ define strips of equal initial masses. The figure provides some interesting clues on the mass of LMC clusters. As an example, if $x = 1.35$, the most luminous young clusters would have initial masses of the same order as the faintest observed old clusters, from 10^4 to 10^5 $M_\odot$. In this scenario, luminous young clusters like NGC 2070, NGC 1850 and NGC 1866 (respectively the brightest clusters in SWB groups 0, II and III) would be the precursors of moderately luminous old clusters as NGC 2257. Luminous classical globular clusters as NGC 1786 and NGC 2210 would have initial masses $\mathscr{M} \sim 10^6$ $M_\odot$, without similar in the recently formed clusters. On the other hand, if $x = 2.5$ the $10^4 < \mathscr{M}(M_\odot) < 10^5$ young clusters would be the direct precursors of the observed old clusters, except for the brightest globulars (e.g. NGC 1835).

In order to check if the present models can consistently reproduce the mass of young and old clusters, Table 1 presents masses and mass-to-light ratios for NGC 1866 (Fischer et al. 1992a; assuming rotational component), NGC 1978 (Meylan et al. 1991; Fischer et al. 1992b) and NGC 1835 (Dubath et al. 1990), based on velocity dispersion measurements. The last two columns of the table give our models' mass-to-light ratios $\mathscr{M}/L_V$. Here $\mathscr{M}$ refers to the *present* cluster mass – i.e., the mass in alive stars and stellar remnants (see Alongi & Chiosi 1989), since a fraction of the initial cluster mass (less than 30%) was expelled by stellar winds and supernovae. For the 10^8 yr model cluster, $\mathscr{M}/L_V$ is by definition equal to that of NGC 1866 (Sect. 2.2). For 10^{10} yr clusters, $\mathscr{M}/L_V$ comes from models based on CCS92 isochrones, which include the He-burning phases. We see that for both xs the models give values encompassing that observed for NGC 1835. For NGC 1978 the $x = 1.35$ model agrees with the Meylan et al. $\mathscr{M}/L_V$ determination, while the $x = 2.5$ model is closer to that of Fischer et al. More clusters with measured velocity dispersion are nec-

Table 1. Observed masses and mass-to-light ratios compared to the model values.

Cluster	t (yr)	source	$\mathcal{M}$ ($M_\odot$)	$\mathcal{M}/L_V$ observed	$\mathcal{M}/L_V$ x=1.35	$\mathcal{M}/L_V$ x=2.5
NGC 1866	$\sim 10^8$	Fischer et al. 1992a	$1.25 \pm 0.25 \times 10^5$	0.19 ± 0.04	0.20	0.20
NGC 1978	$\sim 2 \times 10^9$	Meylan et al. 1991	$0.36 - 1.44 \times 10^6$	$1.2 - 4.2$	2.46	0.79
		Fischer et al. 1992b	$1.3 \pm 0.6 \times 10^5$	0.40 ± 0.15		
NGC 1835	$> 10^{10}$	Dubath et al. 1990	$1.0 \pm 0.3 \times 10^6$	3.4 ± 1.0	10.17	1.48

essary to give statistical significance to conclusions about the IMF slope.

Quantitative information about the rate at which clusters in a certain mass range were created and destroyed can, in principle, be obtained from Fig. 8. We calculated the cluster ADF $\mathrm{d}N_{\rm cl}/\mathrm{d}t$ as a function of $\log t$ in two different ways:

1) The clusters were counted in age bins in mass limited strips as shown in Fig. 8. This could be performed up to $\log t = 8.7$ for $x = 1.35$, and $\log t = 9.3$ for $x = 2.5$, owing to the magnitude cutoff at $V \simeq 13$. The resulting $N_{\rm cl}$ values were divided by the age bin width.
2) All clusters above the $V = 13$ cutoff in Fig. 8 were counted, and corrections were applied to estimate the number of clusters below the cutoff which should be encompassed by a fading line starting at $V = 13$ for the youngest age bin. So, the distribution of the younger clusters is used to estimate the number of unseen clusters for each age bin. It improves the cluster statistics, but may introduce uncertainties because the corrections are increasingly larger for older age bins.

The resulting ADFs, shown in Fig. 9, are essentially the same in the regions not affected by the magnitude cutoff. The last age bin computed with method (1) is already affected by it. As we can see, for $x = 2.5$ the curve $\mathrm{d}N_{\rm cl}/\mathrm{d}t$ seems to decrease monotonically for older ages, while for $x = 1.35$ the curve flattens after ages $10^{8.5}$ yr. In interpreting this behaviour, we have to consider that two factors determine the ADF: the cluster formation rate and the cluster evaporation/dissolution rate.

Taking the ADFs at face values, we can conclude that the cluster formation rate would have increased by about a factor 10 in the last $\sim$ 20 Myr. However, part of this increase can be attributed to the presence of unbound young clusters (i.e. associations) in the sample. Also, there is still a great uncertainty in the models for massive stellar evolution, concerning mainly the mass loss rates and their possible dependence on metallicity, which could affect the shape of the fading lines for these younger ages. Otherwise, we can be confident on the shape of the curves in the interval $7.7 < \log t < 9.4$.

The older clusters may have already lost a significant fraction of their luminosity due to dynamical effects, such as evaporation of stars and/or tidal disruption (Wielen 1988). These effects are certainly important for $t \gtrsim 10^9$ yr, and they might affect considerably the behaviour of $\mathrm{d}N_{\rm cl}/\mathrm{d}t$ for these older ages. However, the ADF decline after $\log t = 8.3$ (SWB IV and later) may indicate that dynamical effects are already acting in shorter timescales. As pointed out by Wielen, it would imply in a high density of objects as massive black holes or giant molecular clouds in the LMC. Alternatively, this decline can represent a real decrease in the cluster formation rate for this age interval.

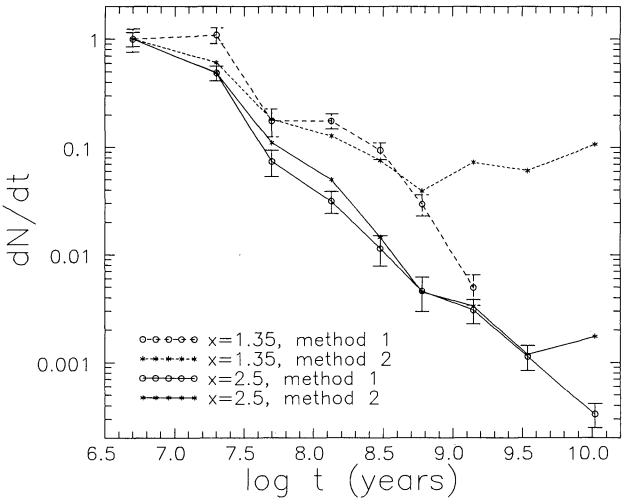

Fig. 9. The cluster age distribution function $\mathrm{d}N_{\rm cl}/\mathrm{d}t$, obtained for the IMF slopes $x = 1.35$ and 2.5, by the two methods described in the text. The curves are normalized at the value for the youngest age bin. Error bars represent the uncertainties due to the counting of clusters

An important point is that the derived cluster ADF is strongly dependent on the adopted IMF slope. Present day observations are not conclusive for its value. Mateo (1988b) derived the value $x = 2.52 \pm 0.16$ in the interval $10.5 > m(M_\odot) > 0.9$ from a group of 6 LMC clusters, a result that was later revised by Richtler et al. (1991), who found $x \simeq 1.3$. Other works (see Conti 1992) found x values from 1.0 to 1.8 for LMC associations. There seems to be a trend for lower x values, $\sim$ 1.35, and indications of cluster-to-cluster variations that can not be neglected. Consequently, these IMF results do not constrain much the ADF scenario.

Our ADFs are smoother than that by Alongi & Chiosi (1991), in which spikes in the derived ADF were associated to periods of enhanced cluster and star formation. The better statistics provided by the larger sample and/or the lower age resolution by the use of SWB groups may be responsible for this difference.

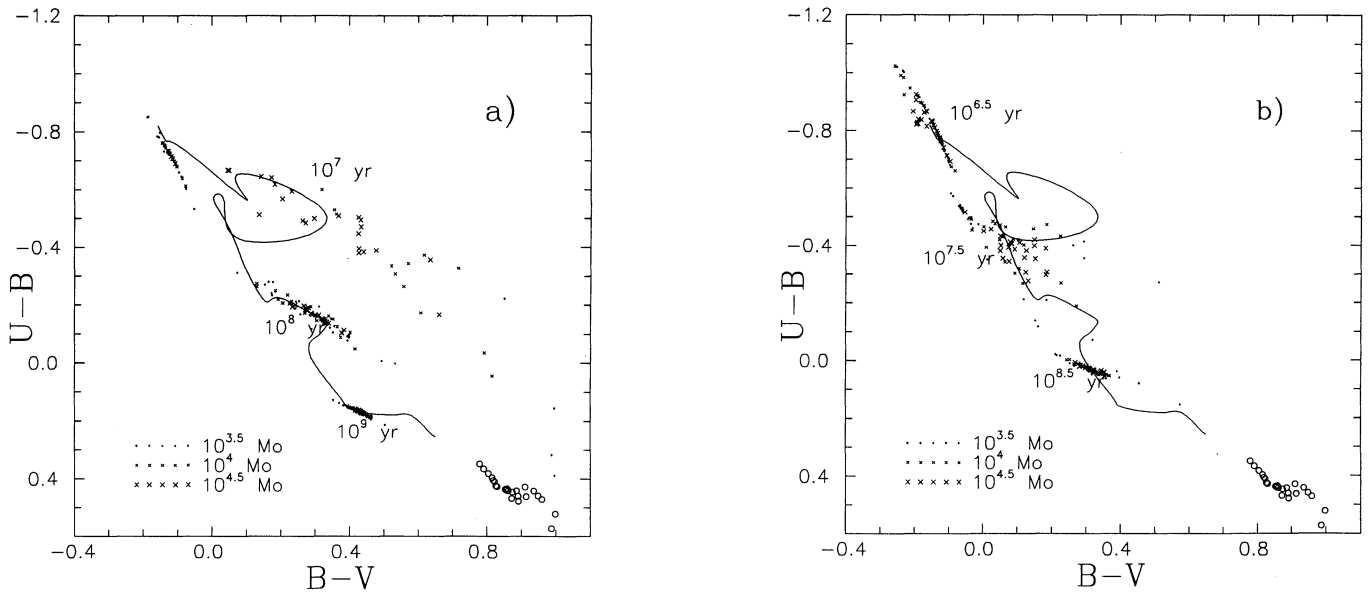

Fig. 10a and b. Dispersion of cluster colours (dots and ×s) caused by stochastic effects on the mass distribution of evolved stars. For x = 2.5, the results are presented for photometric masses $10^{3.5}$, 10^4 and $10^{4.5}$ $M_\odot$, and for ages: **a** 10^7 yr (maximum of RSG phase), 10^8 yr (maximum of 100 Myr red phase) and 10^9 yr; and **b** $10^{6.5}$ yr (in which the evolved stars do not develop red loops), $10^{7.5}$ yr and $10^{8.5}$ yr. The circles present the colour dispersion expected for $10^{4.5}$ $M_\odot$, 4 Gyr model clusters based on CCS92 isochrones

3.2. Stochastic effects on the IMF

The small number of evolved red stars in less populous clusters can cause significant and fast changes in their integrated colours. Works as Barbaro & Bertelli (1977) and CBB88 investigated the magnitude of the dispersion in UBV colours due to these stochastic effects on the stellar mass distribution. Most of the dispersion of points on the $(U-B)$ vs. $(B-V)$ diagram (Fig. 3) can be attributed to it, specially for clusters older than $\sim$ 50 Myr, for which the internal reddening is expected to be negligible. As the dispersion seen in Fig. 3 is clearly variable along the ageing sequence, and as the BCDSP data sample includes fainter clusters than previous ones, we decided to investigate further this point.

3.2.1. The simulations

The following procedure has been followed to simulate the stochastic effects on the IMF. The range of stellar masses in a synthetic cluster was divided into two intervals:

i) The unevolved stars are the stars on the ZAMS, or with a negligible deviation from it. In this mass range, $m < m_{\rm ZAMS}$, the mass spectrum can be considered continuous, because it is far better populated than the subsequent evolutionary stages, and the star colours have a smooth and continuous distribution. The integrated luminosities by unit cluster initial mass were calculated with Eq. (1), and then multiplied by the desired cluster initial mass $\mathscr{M}$.

ii) The evolved stars are the stars in all the subsequent evolutionary stages, covering the range $m_{\rm ZAMS} < m < m_{\rm u}$. It includes sparsely populated stages and with colours and luminosities very deviant from those of the main sequence. So, the presence or not of stars in each evolutionary stage can cause significant changes in the cluster integrated colours. In this mass range, the mass distribution of stars is simulated by a Monte-Carlo integration, in which stellar masses are added one-by-one to the cluster. The probability of occurrence of a given stellar mass is given by the IMF, and the integrated cluster luminosities are increased by the corresponding stellar luminosities. The integration stops when the mass in evolved stars attains the value expected for a cluster with initial mass $\mathscr{M}$.

The only input in the previous procedure are the isochrones and a cluster initial mass $\mathscr{M}$. The latter is chosen such as to cover the range of integrated M_V magnitudes observed (Fig. 8), from ~ -11 to -4 for LMC clusters. Examples of synthetic clusters obtained this way can be seen in Figs. 4 and 5.

The effect is illustrated in Fig. 10, in which we present the dispersion in cluster colours for coeval clusters of photometric masses between $10^{3.5}$ and $10^{4.5}$ $M_\odot$ for some particular ages. For the sake of conciseness, the results are presented only for x = 2.5. A conspicuous effect occurs for very young clusters: those that have no RSG are clumped at very blue colours ($B-V < -0.1$), and those with a small number disperse widely over the $(U-B)$ vs. $(B-V)$ diagram (Fig. 10a). The dispersion increases for lower IMF slopes. After the RSG phase the colour dispersion decreases and becomes almost independent on x. A temporary increase occurs at the 100 Myr red phase. For older clusters, the dispersion occurs along a narrow line, with an inclination $\Delta(U-B) = 0.56\,\Delta(B-V)$ (differing somewhat from that of the reddening vector).

For clusters of equal initial masses, Fig. 10 shows that the general trend is a reduction of the colour dispersion with age,

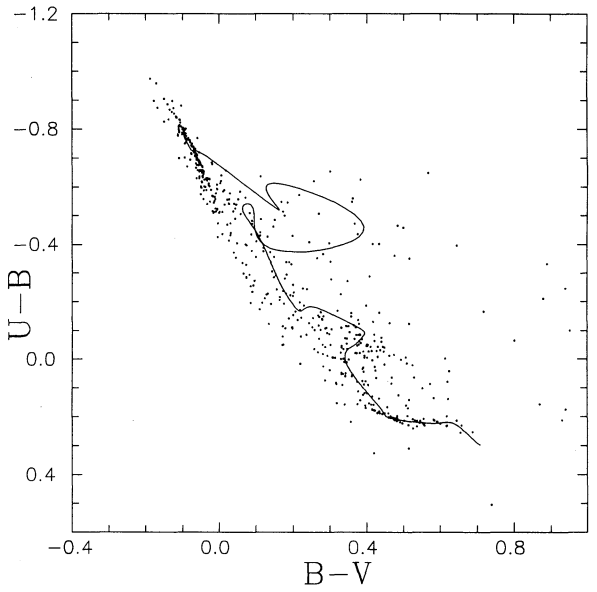

Fig. 11. Simulated $(U-B)$ vs. $(B-V)$ diagram for a set of clusters with the same age and photometric mass distributions as the observed one (Fig. 8)

due to the increasing population of evolved stars. However, the dispersion increases temporarily during the phases with an enhanced population of red stars at 10 and 100 Myr. The same occurs immediately after the RGB phase transition (at $\log t$ = 9.4), when the RGBs are extended. For the case based on CCS92 4 Gyr isochrone, Fig. 10 shows the colour dispersion for $10^{4.5}$ $M_{\odot}$ clusters, which is the mass comparable to the observed old clusters in the sample. Probably the inclusion of TP-AGBs in the model will further increase this dispersion. Indeed luminous carbon stars are observed at the AGB-tip for SWB types V–VI clusters (Frogel et al. 1990).

Figure 11 shows the same kind of simulations, but assuming the same age and photometric mass distributions suggested by Fig. 8. A close comparison of Figs. 11 and 3 shows that:

i) The stochastic effects account well for the observed dispersion for ages $7.5 < \log t < 8.8$. We can notice that the presence of the 100 Myr red phase is responsible for the cluster dispersion at colours $(B-V) \simeq 0.45$, $(U-B) \simeq 0.0$. Models based on classical evolutionary tracks, lacking the 100 Myr red phase, would present a significantly narrower distribution of cluster colours in this age interval.

ii) The dispersion is strongly reduced in the range $8.8 < \log t < 9.4$, because these clusters are already very populous in post-MS stars. It suggests that older clusters, with $(B-V) > 0.6$, would be even less dispersed in the diagram, but they are not (Fig. 3). As already commented, the dispersion is expected to increase after the RGB phase transition due to the presence of extended RGBs and luminous carbon stars at the AGB-tip.

iii) The young clusters observed around the theoretical RSG phase loop are clearly clusters with RSG stars. Simulations for several IMF slopes again show that the observed cluster dispersion is better accounted by $x \simeq 2.5$.

iv) The simulations do not show clusters dispersed on the upper left corner of Fig. 11, while they are seen in Fig. 3 at colours $(B-V) \simeq 0.1$, $(U-B) \simeq -0.9$. However, variable internal reddenings in the very blue clusters (those without RSGs) of the order $E(B-V) \simeq 0.2$ can explain the cluster distribution in this region. Also, the presence of gas emission lines contributes to the dispersion of very young clusters: BCDSP found evidence for the occurrence of a loop in the direction of lower $(U-B)$ values for the clusters associated with bright HII regions.

v) On the other side, the simulations provide a significant number of young clusters with extreme red colours, $(B-V) > 0.6$. They are low luminosity $(V > 12)$ SWB types 0 or I clusters with one or two RSG stars, and no BSGs. The RSG luminosity can even exceed the integrated luminosity due to the other stars. Such extremely red young clusters are not included in BCDSP data. Moreover, many of these small clusters can remain uncatalogued due to selection effects. They can, for example, be confused with single RSGs, as these stars can be 2 or 3 magnitudes brighter than the blue top-MS stars (Fig. 4). Indeed, CCD photometry of bright LMC stars normally reveals the presence of small clusters. Alternatively, RSGs might be considered as non-member stars and excluded from integrated photometries.

3.2.2. The RGB phase transition

Bica et al. (1991) found a gap in the LMC cluster colour distribution at $(B-V) = 0.5$, $(U-B) = 0.1$ (Fig. 3), and interpreted it as being the colour gap caused by the RGB phase transition (Renzini & Buzzoni 1986). In the present models, however, the RGB phase transition occurs at $(B-V) = 0.7$, $(U-B) = 0.2$. This difference is probably due to the different metallicity of the models.

The models provide an interesting possibility: some clusters at the 100 Myr red phase, dispersed by stochastic effects, might enhance the blue side of the gap. Isochrones with a very small age step would be necessary to explore the gap region.

4. Conclusions

The main conclusions of this work are:

1) The presence of the RSG phase at 10 Myr is a well documented observational fact. On the theoretical side, the massive stellar evolution predicts red loops, which however still need further studies as a function of mass loss and metallicity in order to reproduce in detail the observations.

2) Integrated colours are little sensitive to the IMF slope, except for clusters with massive stars. The comparison of the theoretical RSG phase loop in the $(U-B)$ vs. $(B-V)$ diagram with both the distribution of massive clusters observed in the RSG phase by BAS90 (Sect. 2.3.1) and the

observed dispersion of clusters (Sect. 3.2.1) favours steeper IMF slopes ($x \sim 2.0$ to 2.5) for massive stars.

3) Model clusters younger than $\log t \simeq 6.7$ do not have RSGs, so they are clumped at very blue colours. For observed clusters in this age range, internal reddening and the presence of emission lines from the surrounding gas are probably the main sources of colour dispersion. However, small clusters in the RSG phase and later may occupy the same locus owing to the lack of RSGs by stochastic effects.
4) Overshooting tracks provide a temporary red phase at 100 Myr owing to the luminosity and colour evolution of core He-burning stars. An additional colour effect due to cooler stars appears to occur at similar ages (BAS90). Further studies with theoretical colours in the near-IR are necessary to better distinguish these effects.
5) The 100 Myr red phase model clusters, dispersed in integrated colours due to stochastic effects on their IMFs, produce a distribution closely resembling the observed one. Some clusters dispersed to redder colours may reach the blue side of the gap observed at $(B-V) = 0.5$, $(U-B) = 0.1$.
6) The colour evolution of older clusters requires lower metallicity models for a better description of the observations. The colour dispersion due to stochastic effects is expected to increase after the RGB phase transition due to the presence of extended RGBs and carbon stars.

Many aspects of theoretical models are still to be explored to better explain the observations: the inclusion of lower metallicity stellar models, the use of empirical bolometric corrections and colour relations for lower metallicities, a full exploration of the role of overshooting on the occurrence of the 100 Myr red phase, the effect of bimodal IMFs and better age determinations on the cluster ADF derivation.

Acknowledgements. We thank C. Chiosi, G. Bruzual and J.F.C. Santos Jr. for interesting remarks, and A. Maeder and V. Castellani for kindly providing their tracks and isochrones. Financial support from the Brazilian Institution CNPq is also acknowledged.

References

Alongi M., Bertelli G., Bressan A., Chiosi C., 1991, A&A 244, 95
Alongi M., Chiosi C., 1989, in: Astrophysical Ages and Dating Methods, eds. E. Vangioni-Flam et al., Editions Frontières: Gif sur Yvette, p. 207
Alongi M., Chiosi C., 1991, in: The Magellanic Clouds, IAU Symp. 148, eds. R. Haynes and D. Milne, Dordrecht: Reidel, p. 193
Arimoto N., Bica E., 1989, A&A 222, 89
Barbaro G., Bertelli G., 1977, A&A 54, 243
Battinelli P., Capuzzo-Dolcetta R., 1989, ApJ 347, 794
Bertelli G., Bressan A.G., Chiosi C., 1985, A&A 150, 33
Bica E., Alloin D., Santos Jr. J.F.C., 1990, A&A 235, 103 (BAS90)
Bica E., Clariá J.J., Dottori H., Santos Jr. J.F.C., Piatti A., 1991, ApJ 381, L51
Bica E., Clariá J.J., Dottori H., Santos Jr. J.F.C., Piatti A., 1992a, in: The Stellar Populations of Galaxies, IAU Symp. 149, eds. B. Barbuy and A. Renzini, Dordrecht: Kluwer, p. 392 (BCDSP)
Bica E., Clariá J.J., Dottori H., 1992b, AJ 103, 1859
Bruzual G., Charlot S., 1993, ApJ 405, in press.
Buser R., Kurucz R.L., 1978, A&A 70, 555
Carney B.W., Janes K.A., Flower P.J., 1985, AJ 90, 1196
Castellani V., Chieffi A., Straniero O., 1992, ApJS 78, 517 (CCS92)
Charlot S., Bruzual G., 1991, ApJ 367, 126
Chiosi C., Bertelli G., Bressan A., 1988, A&A 196, 84 (CBB88)
Conti P.S., 1992, in: The Stellar Populations of Galaxies, IAU Symp. 149, eds. B. Barbuy and A. Renzini, Dordrecht: Kluwer, p. 93
Dubath P., Meylan G., Mayor M., Magain P., 1990, A&A 239, 142
Elson R.A.W., Fall S.M., 1985, ApJ 299, 211
Fischer P., Welch D.L., Côté P., Mateo M., Madore B.F., 1992a, AJ 103, 857
Fischer P., Welch D.L., Mateo M., 1992b, AJ 104, 1086
Frogel J.A., Mould J., Blanco V.M., 1990, ApJ 352, 96
Johnson H.L., 1966, ARA&A 4, 193
Maeder A., Meynet G., 1989, A&A 210, 155 (MM89)
Maeder A., Meynet G., 1991, A&AS 89, 451 (MM91)
Mateo M., 1988a, in: Stellar Evolution and Dynamics of the Outer Halo of the Galaxy, ESO Workshop 27, eds. M. Azzopardi and F. Matteucci, Garching, p. 467
Mateo M., 1988b, ApJ 331, 261
Mermilliod J.-C, 1981, A&A 97, 235
Meylan G., Dubath P., Mayor M., 1991, in: The Magellanic Clouds, IAU Symp. 148, eds. R. Haynes and D. Milne, Dordrecht: Reidel, p. 211
Renzini A., Buzzoni A., 1986, in: Spectral Evolution of Galaxies, eds. C. Chiosi and A. Renzini, Dordrecht: Reidel, p. 195
Richtler T., de Boer K.S., Sagar R., 1991, The Messenger 64, 50
Sagar R., Richtler T., de Boer K.S., 1991, A&AS 90, 387
Sandage A., 1988, in: Calibration of Stellar Ages, ed. A.G. Davis Philip, L. Davis Press, p. 43
Scalo J.M., 1986, Fund. Cosm. Phys. 11, 1
Schmidt-Kaler T., 1982, Landolt-Börnstein, New Series Group 6, Springer Verlag, Berlin Heidelberg New York, p. 15
Searle L., Wilkinson A., Bagnuolo W.G., 1980, ApJ 239, 803
VandenBerg D.A., Hartwick F.D.A., Dawson P., Alexander D.R., 1983, ApJ 266, 747
van den Bergh S., 1981, A&AS 46, 79
Wielen R., 1988, in: Globular Clusters Systems in Galaxies, IAU Symp. 126, eds. J.E. Grindlay and A.G. Davis Philip, Dordrecht: Reidel, p. 393

This article was processed by the author using Springer-Verlag TEX A&A macro package 1992.